

# Upper Chromospheric Magnetic Field of a Sunspot Penumbra: Observations of Fine Structure

J. Joshi<sup>1,2</sup>, A. Lagg<sup>2</sup>, S. K. Solanki<sup>2,3</sup>, A. Feller<sup>2</sup>, M. Collados<sup>4,5</sup>, D. Orozco Suárez<sup>4,5</sup>, R. Schlichenmaier<sup>6</sup>, M. Franz<sup>6</sup>, H. Balthasar<sup>7</sup>, C. Denker<sup>7</sup>, T. Berkefeld<sup>6</sup>, A. Hofmann<sup>7</sup>, C. Kiess<sup>6</sup>, H. Nicklas<sup>8</sup>, A. Pastor Yabar<sup>4,5</sup>, R. Rezaei<sup>4,5</sup>, D. Schmidt<sup>6</sup>, W. Schmidt<sup>6</sup>, M. Sobotka<sup>9</sup>, D. Soltau<sup>6</sup>, J. Staude<sup>7</sup>, K. G. Strassmeier<sup>7</sup>, R. Volkmer<sup>6</sup>, O. von der Lühe<sup>6</sup>, and T. Waldmann<sup>6</sup>

- <sup>1</sup> Institute for Solar Physics, Department of Astronomy, Stockholm University, AlbaNova University Centre, SE-106 91 Stockholm, Sweden, e-mail: jayant.joshi@astro.su.se  
<sup>2</sup> Max-Planck-Institut für Sonnensystemforschung, Justus-von-Liebig-Weg 3, 37077, Göttingen, Germany  
<sup>3</sup> School of Space Research, Kyung Hee University, Yongin, Gyeonggi Do, 446-701, Republic of Korea  
<sup>4</sup> Instituto de Astrofísica de Canarias (IAC), Vía Lactea, 38200 La Laguna, Tenerife, Spain  
<sup>5</sup> Departamento de Astrofísica, Universidad de La Laguna, 38205 La Laguna, Tenerife, Spain  
<sup>6</sup> Kiepenheuer-Institut für Sonnenphysik, Schöneckstr. 6, 79104 Freiburg, Germany  
<sup>7</sup> Leibniz Institut für Astrophysik Potsdam (AIP), An der Sternwarte 16, 14482 Potsdam, Germany  
<sup>8</sup> Institut für Astrophysik, Georg-August-Universität Göttingen, Friedrich-Hund-Platz 1, 37077 Göttingen, Germany  
<sup>9</sup> Astronomical Institute of the Academy of Sciences, Fričova 298, 25165 Ondřejov, Czech Republic

Received; accepted

## ABSTRACT

**Aims.** The fine-structure of magnetic field of a sunspot penumbra in the upper chromosphere is to be explored and compared to that in the photosphere.

**Methods.** High spatial resolution spectropolarimetric observations were recorded with the 1.5-meter GREGOR telescope using the GREGOR Infrared Spectrograph (GRIS). The observed spectral domain includes the upper chromospheric He I triplet at 10830 Å and the photospheric Si I 10827.1 Å and Ca I 10833.4 Å spectral lines. The upper chromospheric magnetic field is obtained by inverting the He I triplet assuming a Milne-Eddington type model atmosphere. A height dependent inversion was applied to the Si I 10827.1 Å and Ca I 10833.4 Å lines to obtain the photospheric magnetic field.

**Results.** We find that the inclination of the magnetic field shows variations in the azimuthal direction both in the photosphere, but also in the upper chromosphere. The chromospheric variations remarkably well coincide with the variations in the inclination of the photospheric field and resemble the well-known spine and inter-spine structure in the photospheric layers of penumbrae. The typical peak-to-peak variations in the inclination of the magnetic field in the upper chromosphere is found to be 10°–15°, i.e., roughly half the variation in the photosphere. In contrast, the magnetic field strength of the observed penumbra does not show variations on small spatial scales in the upper chromosphere.

**Conclusions.** Thanks to the high spatial resolution observations possible with the GREGOR telescope at 1.08 microns, we find that the prominent small-scale fluctuations in the magnetic field inclination, which are a salient part of the property of sunspot penumbral photospheres, also persist in the chromosphere, although at somewhat reduced amplitudes. Such a complex magnetic configuration may facilitate penumbral chromospheric dynamic phenomena, such as penumbral micro-jets or transient bright dots.

**Key words.** Sun: magnetic field - Sun: activity - Sun: chromosphere - Sun: infrared - Techniques: polarimetric - Techniques: spectroscopic

## 1. Introduction

In photospheric layers, the magnetic field of sunspot penumbrae possesses a highly complex structure, varying in both, strength and orientation on fine spatial scales. It is organized in nearly radially aligned filaments (at least in the inner penumbra) where strong and weak magnetic fields are alternatingly present in azimuthal direction. Similarly, the magnetic field orientation is organized in vertical (spines) and horizontal (inter-spines) components (Schmidt et al. 1992; Title et al. 1993; Solanki & Montavon 1993; Martínez Pillet 2000; Langhans et al. 2005; Scharmer & Henriques 2012; Tiwari et al. 2013). Relations between various physical parameters of penumbrae, such as the magnetic field strength, field orientation, brightness and plasma flows (Ever-

shed effect), have been studied for the last few decades, leading to some controversial results (for detailed reviews on the topic see, e.g., Solanki 2003; Borrero & Ichimoto 2011; Rempel & Schlichenmaier 2011). A recent study by Tiwari et al. (2013) seems to settle most of the controversies and presented a uniform picture of penumbral filaments. They conclude that the penumbral filaments harbor a comparatively weak horizontal magnetic field except at its head, where the field is relatively vertical, and at tail, where the field has opposite polarity. Such filaments are, at least in the inner part of the penumbra embedded in strong and less inclined background magnetic field.

Another feature of the photospheric penumbral magnetic field is the presence of opposite polarity patches (compared to the polarity of the umbra) at the tails and edges of penumbral

filaments (Scharmer et al. 2013; Ruiz Cobo & Asensio Ramos 2013; Franz & Schlichenmaier 2013; Tiwari et al. 2013; van Noort et al. 2013; Joshi 2014; Joshi et al. 2016b). These opposite polarity patches are thought to originate from advection of penumbral field by overturning convection. The presence of overturning convection in penumbrae has been successfully observed (Joshi et al. 2011; Scharmer et al. 2011; Tiwari et al. 2013; Esteban Pozuelo et al. 2015).

The chromosphere and transition region above the sunspot penumbrae display dynamics on arcsec and sub-arcsec scales, such as penumbral micro-jets (Katsukawa et al. 2007; Jurčák & Katsukawa 2008; Reardon et al. 2013; Vissers et al. 2015; Tiwari et al. 2016) and transient bright dots (Tian et al. 2014). Katsukawa et al. (2007) suggest reconnection between two magnetic components (spines and inter-spines) as a driver of penumbra jets, whereas Tiwari et al. (2016) argued for reconnection between opposite polarity patches and fields from spines (cf. Magara 2010). Tian et al. (2014) also speculate that bright dots they observed in the penumbra may originate from heating of plasma to transition region temperature due to reconnection of magnetic fields from spine and inter-spine regions. In literature small-scale transient events in the chromosphere and transition region above sunspot penumbrae are usually linked to the complex magnetic structure in the photosphere. Does the chromospheric magnetic field of penumbrae play any role in these dynamics? This topic has not been investigated because information about the magnetic field fine structure of sunspots at chromospheric heights is lagging behind that in the photosphere, especially in terms of spatial resolution. The general structure of sunspot magnetic fields has been studied by Rüedi et al. (1995), Joshi (2014), Schad et al. (2015) and Joshi et al. (2016a) by using observation in the He I triplet at 10830 Å.

In this paper, we present the first high spatial resolution maps of the penumbral magnetic field in the upper chromosphere obtained from the He I triplet at 10830 Å observed with the 1.5-meter GREGOR telescope.

## 2. Observations

We observed a part of a sunspot penumbra in the active region NOAA 12096 on 25 June 2014 with the 1.5-meter GREGOR telescope (Schmidt et al. 2012). Spectropolarimetric observations were recorded with the GREGOR Infrared Spectrograph (GRIS, Collados et al. 2012) combined with the Tenerife Infrared Polarimeter-2 (TIP-2, Collados et al. 2007). The GREGOR telescope is equipped with the GREGOR Adaptive Optics System (GAOS, Berkefeld et al. 2012; Berkefeld et al. 2010) which worked during the observations under good seeing conditions.

We observed a 18 Å wide range centered around 10833 Å with a spectral sampling of 18 mÅ. The observed field-of-view (FOV) was obtained by a raster scan of the 63"3 long slit with 60 steps, and a step size of 0"135. The pixel size along the slit is 0"135. Full Stokes profiles were recorded with an exposure time of 40 ms, with ten accumulations for every Stokes parameter. The heliocentric coordinates of the centers of the observed FOV were (7°N, 38°E), so that the cosine of the heliocentric angle is  $\mu = 0.78$ .

Standard data reduction steps have been applied to the raw data (see Collados et al., in preparation), which encompass procedures such as, corrections for dark current and flat-field, removal of geometrical distortions and fringes as well as polarimetric calibration and cross-talk removal. The continuum level was corrected using a Mcath-Pierce Fourier Transform Spec-

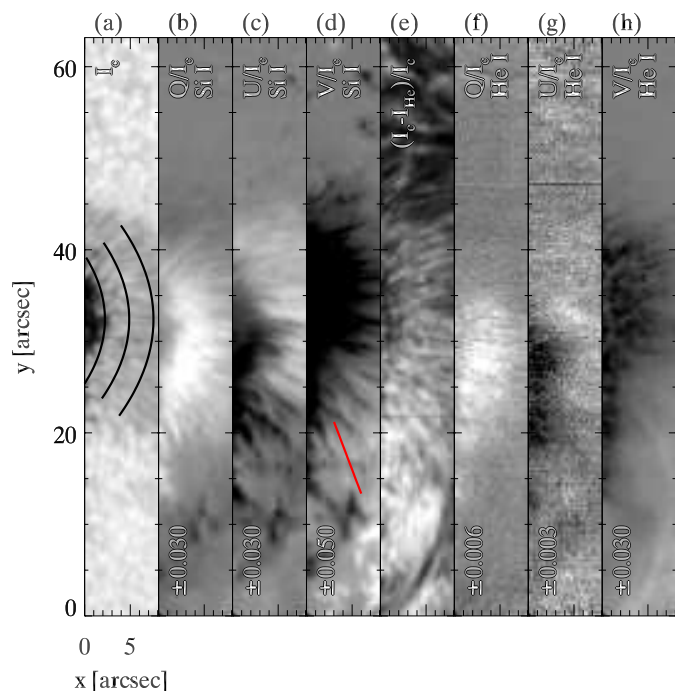


**Fig. 1.** Maps of Stokes parameters for the Si I 10827.1 Å line and the He I triplet at 10830 Å. Panel (a) shows continuum intensity,  $I_c$ , at 10833 Å. Panels (b), (c) and (d) corresponds to Stokes  $Q/I_c$ ,  $U/I_c$  and  $V/I_c$  maps of the Si I line, respectively. The line depression of the blended red components of the He I triplet,  $(I_c - I_{He})/I_c$ , is displayed in panel (e). Stokes  $Q/I_c$ ,  $U/I_c$  and  $V/I_c$  maps for the He I triplet are presented in panels (f), (g) and (h), respectively. The lower and upper limits of the Stokes  $Q/I_c$ ,  $U/I_c$  and  $V/I_c$  maps are indicated in the lower part of the respective image. The Stokes maps presented here are an average over a 0.27 Å wide range centered at  $\lambda - \lambda_0 = -3.10$  Å and  $\lambda - \lambda_0 = -0.35$  Å for the Si I line and He I triplet, respectively, with  $\lambda_0 = 10830$  Å. Stokes  $V/I_c$  profiles along the red line marked in panel (d) are plotted in Fig. 2. The lower part of the line is directed towards the closest part of the solar limb. Three arcs in panel (a) show the locations of various parameters which are depicted in Fig. 6.

trometer (FTS) spectrum (Livingston & Wallace 1991; Wallace et al. 1993). The spectral resolution of the recorded spectra is estimated in a similar way as in Borrero et al. (2016) by least-square fitting the FTS spectrum convolved with a Gaussian spectral point-spread-function (PSF) to the averaged quiet-Sun spectrum (recorded in flat-field mode on the disk center). The best fit between the FTS and averaged quiet Sun spectrum is found for a PSF with FWHM = 120 mÅ and a spectral straylight of 14%. This value of FWHM corresponds to a spectral resolution of  $\lambda/\Delta\lambda \approx 90,000$ , which is similar to that found by Borrero et al. (2016) for the GRIS/GREGOR observations recorded at 1.56 μm (also see, Franz et al. 2016).

We estimated the spatial resolution of the observations to be  $\sim 0"35$  by looking at the spatial power spectrum. For comparison, the diffraction limited resolution of the GREGOR at 10832 Å is  $\sim 0"18$ , and the best resolution that GRIS can achieve at this wavelength is  $\sim 0"27$  (twice the pixel size). To improve the signal-to-noise ratio of Stokes parameter we binned data by two pixels both in the slit direction and the scanning direction (effective spatial resolution  $\sim 0"54$ ) as well as three pixels in the direction of spectral dispersion. This implies reducing the spatial resolution somewhat, but greatly enhances the signal-to-noise ratio of the data, allowing for much more reliable maps of the magnetic vector in the chromosphere. Figure 1 presents the

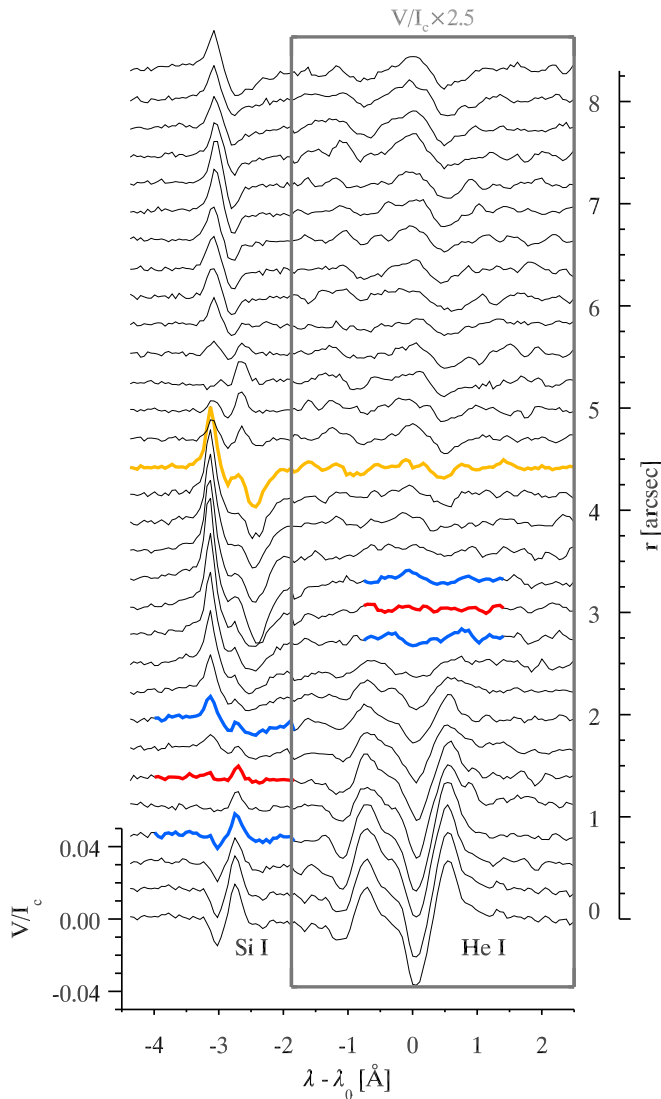


**Fig. 2.** Stokes  $V$  profiles over a spectral range covering the Si I 10827.1 Å line and He I triplet at 10830 Å. Positions of the plotted profiles are indicated by a red line in Fig. 1(d), the lowermost profile belongs to the pixel closest within the sunspot to the sunspot center. Since the Stokes  $V$  signal in the He I triplet is weaker compared to the Si I line, it is magnified by a factor of 2.5 (see box). The axis right side of the plot gives the distance,  $r$ , in seconds of arc from the lowermost profile. Profiles plotted in red indicate the position of the polarity inversion line and those colored in blue indicate the nearest profiles with clearly visible opposite polarity. A yellow profile at  $r = 4.5$  marks the transition from the penumbral region to the quiet Sun.

observed continuum intensity,  $I_c$ , at 10833 Å over the observed FOV (panel (a)), line depression of the blended red components of the He I triplet at 10830 Å,  $(I_c - I_{He})/I_c$  (panel (e)). Stokes  $Q$ ,  $U$  and  $V$  maps for the Si I 10827.1 Å line are shown in panels (b)–(d) and those for the He I triplet are displayed in panels (f)–(h).

### 3. Inversions

#### 3.1. The He I 10830 Å triplet

The He I triplet at 10830 Å originates from the transition between the lower  $1s2s\ ^3S_1$  and the upper  $1s2p\ ^3P_{0,1,2}$  energy levels, generating three spectral lines: a blue component at

10829.09 Å and two blended red components at 10830.30 Å. The He I triplet is strongly influenced by EUV coronal irradiation, capable of ionizing neutral helium atoms, which then, by recombination processes, populate the lower level of the transition (Avrett et al. 1994; Andretta & Jones 1997; Centeno et al. 2008; Leenaarts et al. 2016).

The He I triplet is thought to be formed near the top of the chromosphere because the UV radiation does not penetrate deep into the chromosphere, populating the ground state of the He I triplet only in the upper layers. We inverted the He I triplet to obtain the upper chromospheric magnetic field and the Doppler velocities with the HeLix<sup>+</sup> (Lagg et al. 2004, 2009) inversion code assuming a Milne-Eddington type model atmosphere which has proved to be a reasonable approximation for the He I triplet. We used eight free parameters in the model atmosphere to fit the observed Stokes profiles in the He I triplet: magnetic field strength, inclination and azimuth of the magnetic field vector, the Doppler velocity, the Doppler broadening, the damping constant, gradient of the source function and the ratio between line-center and the continuum opacity. The Si I 10827.1 Å line blends with the blue component of the He I triplet. To take this blend into account we also fit the Si I line, together with the He I triplet (for more details see Joshi et al. 2016b).

#### 3.2. The Si I 10827.1 Å and Ca I 10833.4 Å lines

To retrieve the height-dependent photospheric atmosphere, simultaneous inversions of the Si I 10827.1 Å and Ca I 10833.4 Å lines are performed to satisfy the radiative transfer equation (RTE) under the assumption of local thermodynamic equilibrium (LTE). We used the SPINOR inversion code (Frutiger et al. 2000) which is based on the STOPRO routines (Solanki 1987). We used the same set of line parameters as used by Joshi et al. (2016b).

The model atmosphere used to fit the observed Stokes profiles of the Si I and Ca I lines consists of the temperature, the Doppler velocity, the magnetic field strength, inclination and azimuth as free parameters at three nodes,  $\log \tau_{1083} = 0.0, -0.7, -2.3$ . The micro- and macro-turbulence are assumed to be constant with height. Here  $\tau_{1083}$  denotes the optical depth at 1083 nm. The node positions are chosen based on the analysis of the magnetic field response function as carried out by Joshi et al. (2016b) (also see Chapt. 4 of Joshi 2014) for the lines under consideration.

We are aware of the fact that the Si I 10827.1 Å line-core forms under non-local thermodynamic equilibrium (NLTE) conditions (see Bard & Carlsson 2008). Kuckein et al. (2012) have demonstrated that the temperature is the most affected atmospheric parameter when NLTE is not taken into account for the synthesis of this line. The effect on the magnetic field and Doppler velocities is negligible. In this paper, we only discuss the magnetic field and Doppler velocities, justifying the assumption of LTE.

The spectral PSF (plus spectral straylight, 14%) of the observations is self-consistently included in the SPINOR and HeLix<sup>+</sup> inversions. We have not included the spatial PSF of the GREGOR and also ignored spatial straylight in the inversions. This washes out contrasts, but should not affect our results qualitatively.

### 4. Formation height of the He I triplet

Stokes  $V$  profiles of sunspots observed away from the disk center in a photospheric and a chromospheric spectral line provide a



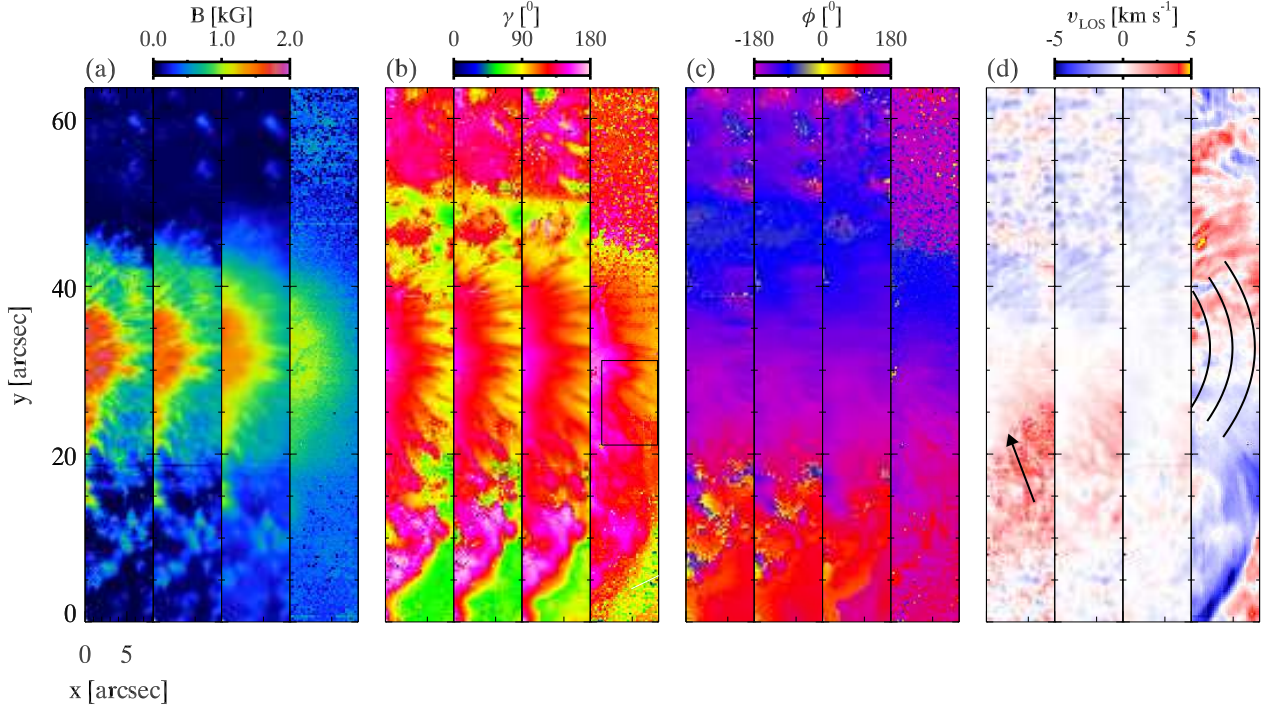


**Fig. 3.** Maps of the magnetic field vector (from left to right: magnetic field strength,  $B$ , inclination,  $\gamma$ , azimuth,  $\phi$ ) and LOS-velocity,  $v_{\text{LOS}}$ , in the photosphere and upper chromosphere. The first three maps in every panel correspond to  $\log \tau = 0.0$ ,  $\log \tau = -0.7$  and  $\log \tau = -2.3$  (SPINOR inversion of the Si I and Ca I lines), and the fourth map refer to the upper chromosphere (HeLIx<sup>+</sup> inversion of the He I triplet). The box in the fourth map of the panel (b) represents the location for which details of various parameters are displayed in Fig. 4. Three arcs in panel (d) show the locations of various parameters which are depicted in Fig. 6 and 7. An arrow in panel (d) indicates the disk center direction.

good opportunity to estimate the difference in formation heights of the lines. Line-of-sight (LOS) magnetograms of sunspots observed away from disk center show an apparent neutral line (reversal of polarity) typically located on the limb side of their penumbra. The exact position of the neutral line with respect to the center of the sunspot depends on the view angle and the orientation of the penumbral field. In the typical magnetic field configuration of a sunspot with field lines expanding with height, the Stokes  $V$  profiles along the line-of-symmetry (the line joining the disk center and sunspot center) change sign at the location where the magnetic field is perpendicular to the LOS. The He I triplet forming higher in the atmosphere, has its neutral line shifted towards the limb compared to that for the lower forming Si I 10827.1 Å line. Knowing the separation between the neutral lines,  $\Delta r$ , and the viewing angle,  $\theta$ , one can obtain a rough estimate of the difference in the formation heights,  $\Delta h$ , using the following formula,

$$\Delta h = \frac{\Delta r}{\tan \theta}, \quad (1)$$

under the assumption that the polarity inversion line lies at about the same location when projected on the solar surface at both heights. This is the case if the magnetic field (after spatially averaging away the fine structure) at both heights has roughly the same inclination to the vertical (see discussion below).

Figure 2 shows Stokes  $V$  profiles both for the Si I 10827.1 Å line and the He I triplet along the line-of-symmetry crossing the neutral line. The bottom-most and top-most profiles are located towards the sunspot center and limb, respectively. Profiles colored in blue show the location of the two nearest Stokes  $V$

profiles with opposite sign, whereas profiles in red color identify the location of the polarity inversion lines. It is evident that the polarity inversion line for the He I triplet appears closer to the limb compared to that for the Si I 10827.1 Å line. The separation between the neutral lines is  $\sim 1''.62$ , which is equal to  $\sim 1530$  km after correcting for the foreshortening. Therefore, according to Eq. 1, the difference in formation height should be around 1900 km, but Eq. 1 is valid only when the magnetic field orientation with respect to the LOS is the same at both heights. The inclination of the magnetic field obtained from the He I triplet, however, is on average  $12^\circ$  more vertical compared to the inclination in the photosphere (see Joshi 2014; Joshi et al. 2016a, and Sect. 5 of this article). After including (adding to  $\theta$ ) this difference of the inclination angle into the Eq. 1, the difference between the formation height of the He I triplet and Si I line is reduced to around 1250 km. Note that the formation height derived here is specific to the sunspot penumbra and may differ significantly in other solar features.

The Si I 10827.1 Å line has multi-lobe Stokes  $V$  profiles at and close to the periphery of the sunspot ( $r = 4''.5 - 5''.5$ ), similar to those close to the polarity inversion line ( $r = 1''.5$ ). But, the multi-lobe Stokes  $V$  profiles at the periphery of the sunspot are most probably due to unresolved mixed polarities or due to a steep gradient in the inclination of the magnetic field with height just outside the sunspot. The He I triplet displays normal Stokes  $V$  profiles at these locations, indicating that any disturbance to the field is restricted to layers below its formation height.

## 5. Results

Maps of the magnetic field vector and LOS-velocity obtained for the photosphere and upper chromosphere are displayed in

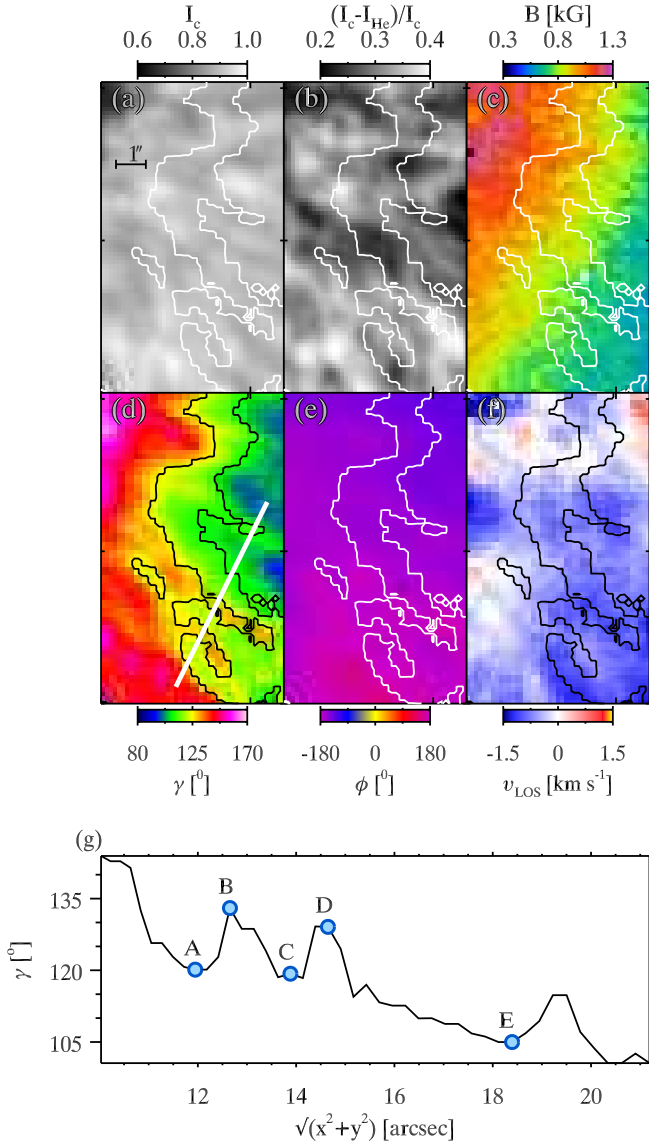


**Fig. 4.** Details of penumbral fine structure in the upper chromosphere. (a)  $I_c$ , (b)  $(I_c - I_{He})/I_c$ , (c)  $B$ , (d)  $\gamma$ , (e)  $\phi$  and (f)  $v_{LOS}$ . The location of the maps is indicated by a box in the fourth map of Fig. 3(b). Contours in panels (a)–(f) depict  $\gamma = 110^\circ, 125^\circ$ . Panel (g) depicts variations in  $\gamma$  along the white line marked in panel (d). Blue circles identified as A–E in panel (g) represent locations of observed and synthesized Stokes profiles of the He I triplet plotted in Fig. 5.

Fig. 3. The first three maps in each panel correspond to parameters at  $\log \tau = 0.0$ ,  $\log \tau = -0.7$  and  $\log \tau = -2.3$  obtained by SPINOR inversions of the Si I 10827.1 Å and Ca I 10833.4 Å lines. The fourth map in each panel is for the parameters returned by HeLIx<sup>+</sup> inversions of the He I 10830 Å triplet. The presented magnetic field vectors are transformed from the LOS frame of reference to the solar frame of reference using a transformation matrix provided by Wilkinson et al. (1989). Before the transformation, the 180° ambiguity in the azimuth direction of the magnetic field was resolved using the “acute angle” method (Sakurai et al. 1985; Cupperman et al. 1992). The LOS-velocities are calibrated by setting the average umbral velocity at  $\log \tau = 0$  to zero.

All three nodes in the photosphere show the same variation in the magnetic field strength in the azimuthal direction. These alternating weak and strong field structures are aligned nearly

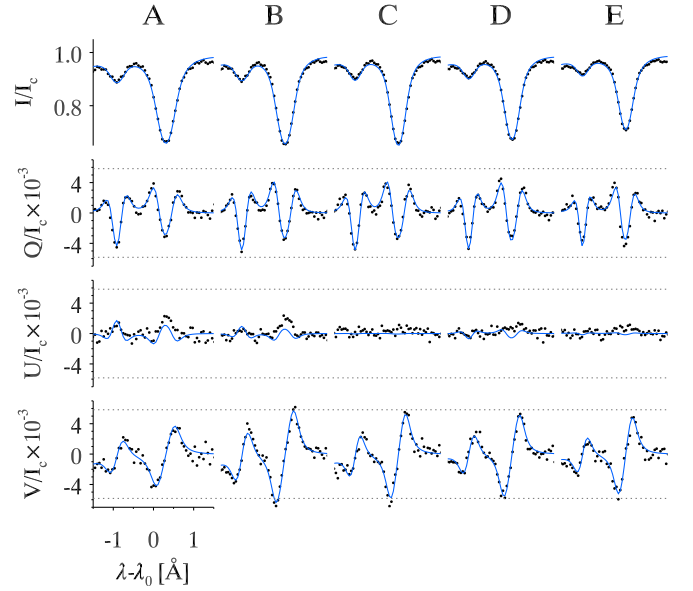


**Fig. 5.** Observed (black dots) and synthesized (blue curves) Stokes profiles. The computed, blue profiles were obtained by the inversions of the He I triplet. Positions of columns named A–E are marked in Fig. 4(g).

in the radial direction. In a similar way, the inclination of the magnetic field is structured, where the relatively horizontal and vertical fields are organized in the same filamentary structure. The upper chromosphere magnetic field strength does not display any variation in azimuthal direction, but the inclination of the field does exhibit such a variation in the azimuthal direction which is qualitatively similar to that in the photosphere. The LOS velocities in the photosphere show clear patterns of the radially outward directed Evershed flow, with decreasing velocities from  $\log \tau = 0.0$  to  $\log \tau = -0.7$ , and velocities close to zero at  $\log \tau = -2.3$ . In the upper chromosphere, the LOS-velocities have the opposite sign to that in the photosphere, displaying the inverse Evershed flow.

A blow-up of the upper chromospheric magnetic field and LOS-velocity maps corresponding to the location indicated by a box in Fig. 3(b) is presented in Fig. 4. The filamentary structure is apparent in the inclination, but not in the magnetic field strength. Contours of the inclination are plotted over the maps of  $I_c$ ,  $(I_c - I_{He})/I_c$ ,  $B$ ,  $\phi$  and  $v_{LOS}$  in panels (a)–(d) and (f) of Fig. 4, respectively. These contours suggest that the small-scale structures in the inclination map do not have a one-to-one correspondence with any of these parameters.

To check the reliability of the small-scale filamentary structure found in the inclination at upper chromospheric heights from the inversions of the He I 10830 Å triplet, it is important to evaluate the quality of the fits to the observed Stokes profiles. Figure 4(g) depicts the variation in the inclination of the magnetic field along a line plotted in panel (d) of Fig. 4. To demonstrate the quality of the fits, we choose multiple locations (marked as A–E in Fig. 4(g)) along this line where the relatively horizontal and vertical field lines appear close to each other and present the corresponding observed and synthesized Stokes profiles in Fig. 5. The match between the observed and synthesized Stokes profiles is exceptionally good for all locations. The variation in the amplitudes of the Stokes profiles also support the variation in the inclination obtained through the inversions. For example, locations-A and -B have similar amplitudes in Stokes  $Q/U$ , but the Stokes  $V$  amplitude at location-B is larger than that

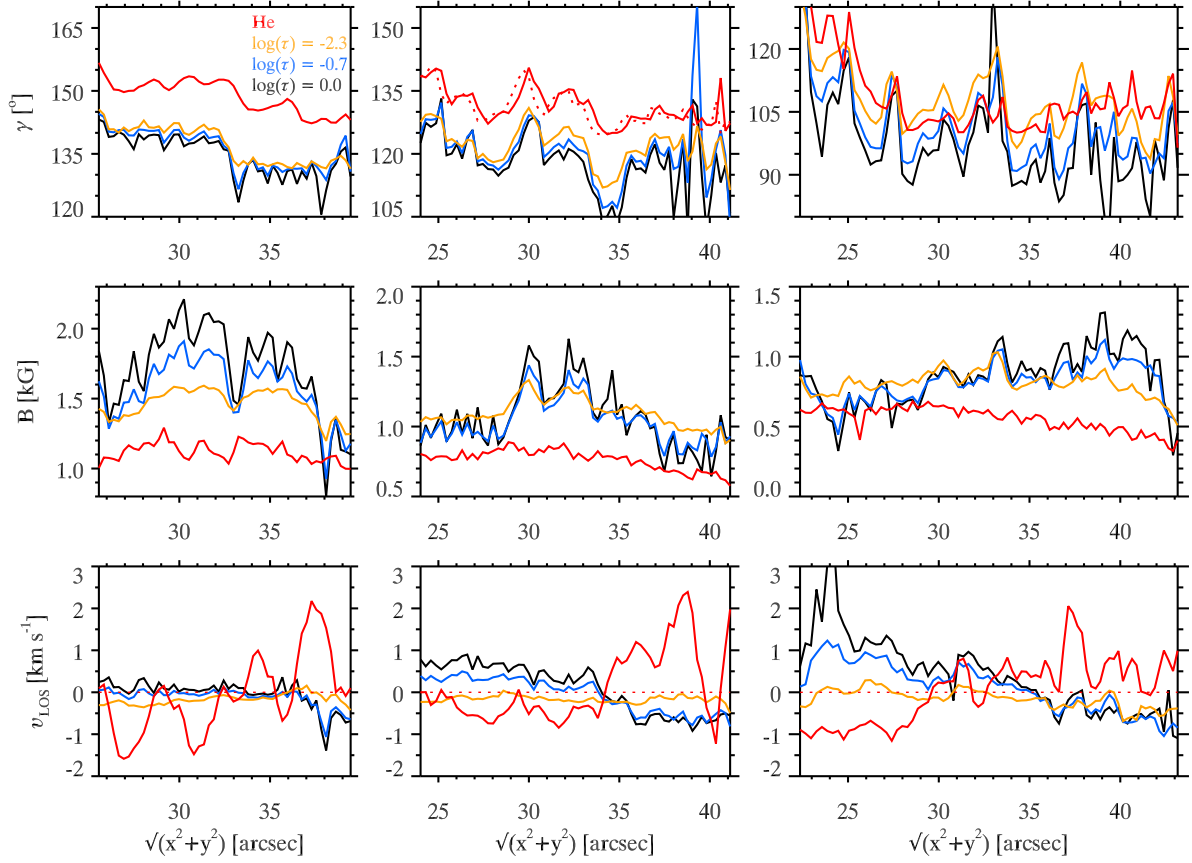


**Fig. 6.** Profiles of the inclination of magnetic field,  $\gamma$  (top row), the magnetic field strength,  $B$  (middle row) and the LOS-velocity,  $v_{\text{LOS}}$  (bottom row), along the arcs (see Fig. 1(a)) at the umbra-penumbra boundary (left column), middle penumbra (middle column) and outer penumbra (right column). Black, blue, yellow and red curves correspond to  $\log \tau = 0.0, -0.7, -2.3$ , and the upper chromosphere, respectively. All the upper chromospheric parameters are plotted after correcting for the shift due to viewing angle and formation height. To illustrate this shift, an uncorrected profile is displayed by the dashed red line in the middle panel of the top row. The left of a panel corresponds to the bottom of the respective arc.

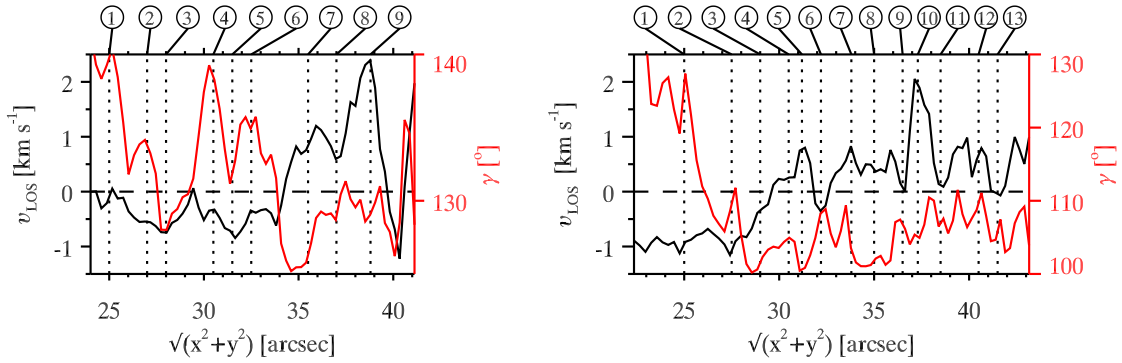


**Fig. 7.** Variations of the LOS-velocity,  $v_{\text{LOS}}$  (black curve), and inclination of the magnetic field  $\gamma$  (red curve) obtained from the He I triplet, along middle (left panel) and outer (right panel) arcs shown in Fig. 1(a). Numbered vertical lines in both panels represent the locations of which variations of  $v_{\text{LOS}}$  and  $\gamma$  are discussed in Sect. 5.

at location-A, suggesting a more vertical field at location-B, similar to the results of the inversions.

For a qualitative comparison between the photospheric and upper chromospheric magnetic field and the LOS-velocity we depict the parameters in Fig. 6 along three arcs (see Fig. 1(a)) located at the umbra-penumbra boundary, the middle and outer penumbra, respectively. Due to the viewing angle (away from disk center) and the difference in the formation height (1250 km) between the Si I line and the He I triplet, parameter maps in the upper chromosphere are shifted by projection towards the limb compared to those in the photosphere. The profiles of the atmo-

spheric parameters plotted in Fig. 6 are corrected for this shift. The inclination of the magnetic field along the arc at the umbra-penumbra boundary does not show much variation, both in the upper chromosphere and photosphere. In the middle and outer penumbra, a variation in the inclination angle due to spines (vertical field) and inter-spines (horizontal field) is seen at all plotted photospheric heights. These variations in the photospheric inclination coincide with that in the upper chromosphere. Peak-to-peak variation in the inclination decreases from  $20^\circ$ – $25^\circ$  at  $\log \tau = 0.0$  to  $\log \tau = -2.3$  and reach their lowest value of  $10^\circ$ – $15^\circ$  in the upper chromosphere. At a few locations in the outer-



most arc, the magnetic field has an inclination less than  $90^\circ$  at  $\log \tau = 0.0$ , i.e., these locations have opposite polarity compared to the umbra. Overall the magnetic field becomes more vertical with height in the photosphere, and in the upper chromosphere it becomes even more vertical by an average angle of  $12^\circ$  compared to that at  $\log \tau = 0.0$ .

The magnetic field strength shows variations due to spines and inter-spines at  $\log \tau = 0.0$  along all the arcs in the penumbra. These variations in the field strength decrease at  $\log \tau = -0.7$  and  $\log \tau = -2.3$  and completely vanish at the upper chromosphere. Some parts (mostly at inter-spines and at their edges) of the arcs in the middle and outer penumbra have a higher magnetic field strength at  $\log \tau = -0.7$  and  $\log \tau = -2.3$  than at  $\log \tau = 0.0$ .

The gas in the arc at the umbra-penumbra boundary is nearly at rest along the LOS at all the photospheric heights, while in the upper chromosphere, the velocity fluctuate strongly, with multiple locations of upflows and downflows (also see Fig. 3). The middle and outer arc indicate small-scale variations in the inverse Evershed flow at chromospheric height. To investigate the relation between these small-scale variations and the inclination angle of the magnetic field, if there is any, we plot both quantities along the middle and outer arc in Fig. 7. Both panels in Fig. 7 suggest that the inverse Evershed flow and the inclination have variations on similar spatial scales. There are some hints that the stronger flows corresponds to the more horizontal magnetic field and the more vertical field has weaker flows (see for example 1<sup>st</sup>, 3<sup>rd</sup> – 7<sup>th</sup> and 8<sup>th</sup> dotted vertical line in the left panel and 5<sup>th</sup> – 9<sup>th</sup> line in the panel on the right in Fig. 7). However, this relation between the inclination of the field and inverse Evershed flow is not particularly robust and is not present at all locations.

## 6. Summary and Discussions

We have presented the magnetic field structure of a sunspot penumbra in the upper chromosphere at high spatial resolution and have compared it with that in photospheric layers. In the photospheric layers the well-known spine and inter-spine structure of penumbrae in the inclination of the magnetic field are clearly visible in our data (Lites et al. 1993; Title et al. 1993; Solanki & Montavon 1993; Martínez Pillet 2000; Langhans et al. 2005; Scharmer et al. 2013; Tiwari et al. 2013). Our analysis reveals that the spine and inter-spine structure is more prominent at  $\log \tau = 0$  than at  $\log \tau = -0.7, -2.3$ , in agreement with results of Borrero et al. (2008), Scharmer et al. (2013) and Tiwari et al. (2013). The striking result obtained here are the observation of variations in the magnetic field inclination in the upper chromosphere. Such variations are most prominent along a cut in the azimuthal direction around the sunspot, and they resemble the spine and inter-spine structure in the photosphere. Our analysis reveals that these variations in the upper chromosphere coincide remarkably well with those in the photosphere, with typical peak to peak variations in the inclination of the field of  $10^\circ$ – $15^\circ$ , compared to  $20^\circ$ – $25^\circ$  at  $\log \tau = 0$ .

A radially aligned filamentary structure in the magnetic field strength is also visible in our results at all photospheric layers with decreasing variation with height. The upper chromospheric map of magnetic field strength does not show any significant variation in the lateral direction, but only a monotonic decrease from the inner to outer penumbra (also see, Joshi 2014; Schad et al. 2015). The absence of fine structure in the magnetic field strength map of the penumbra at the upper chromosphere is probably due to the dominance of magnetic pressure over gas pressure at this height and the absence of significant turbulence, contrary to the turbulent photosphere with high plasma- $\beta$  (ratio

of plasma pressure to magnetic pressure), where the magnetic field gets structured on fine spatial scale. The presence of spine and inter-spine structure found in the maps of magnetic field inclination in the upper chromosphere suggest that the orientation of field lines at the photospheric heights is preserved by some extend up to  $\sim 1250$  km above the formation height of the Si I 10827.1 Å line.

The observed variations in the magnetic field inclination in the lateral direction might be underestimated at the upper chromospheric height due to the limited resolution of our data. This speculation arises from the fact that our results do not show opposite polarity (compared to magnetic polarity in the umbra) lanes as observed by Scharmer et al. (2013), Ruiz Cobo & Asensio Ramos (2013) and Tiwari et al. (2013) at the edges of penumbral filaments in the photosphere. This is because our observations have a lower resolution compared to the observations analyzed in the above studies. Also, overlooking of the spatial PSF and stray-light may contribute to underestimating in the variations of the inclination of the magnetic field. However, we do observe some opposite polarity patches at the tails of penumbral filaments at  $\log \tau = 0$ , similar to those observed by Ruiz Cobo & Asensio Ramos (2013), Franz & Schlichenmaier (2013), Scharmer et al. (2013) and Tiwari et al. (2013). Finally, our study also confirms the localized presence of a negative vertical gradient of the magnetic field strength in the photospheric layers of the penumbra, i.e., magnetic field strength decreases with depth as reported by Tiwari et al. (2015) and Joshi et al. (2016b). The latter authors interpreted the observed negative vertical gradient as a result of the strong magnetic field from spines closing above the weaker field inter-spines and also as a result of unresolved opposite polarity patches in the deep photosphere.

The magnetic field strength, in general, decreases with height in the photosphere and into the upper chromosphere. The average magnetic field strength close to the inner and outer penumbra is around 1.7 kG and 0.8 kG in the photosphere ( $\log \tau = 0.0$ ), respectively, and 1.05 kG and 0.55 kG in the upper chromosphere. If we use the difference between the formation height of the Si I 10827.1 Å line and the He I triplet of 1250 km that we have determined, the vertical gradient turns out to be  $\sim 0.6 \text{ G km}^{-1}$  and  $\sim 0.2 \text{ G km}^{-1}$  in the inner and outer parts of the penumbra, respectively. The difference in the formation height of the Si I line and the He I triplet is estimated using the separation between the polarity-inversion lines displayed by these spectral lines. These values of the vertical gradient of the magnetic field strength are similar to those reported earlier using the same spectral lines (see Rüedi et al. 1995; Joshi 2014; Schad et al. 2015; Joshi et al. 2016a). Our results indicate that in general the magnetic field of the penumbra becomes more vertical with height in the photosphere (also see Borrero & Ichimoto 2011; Tiwari et al. 2013) and in the upper chromosphere it is more vertical by  $\sim 12^\circ$  compared to that in the photosphere ( $\log \tau = 0.0$ ). This difference in the magnetic field inclination between the photosphere and upper chromosphere is similar to that found by Joshi (2014) and Joshi et al. (2016a).

In summary, we report, to our knowledge, the first observations of fine structure of the penumbral magnetic field of a sunspot in the upper chromosphere, which displays lateral variation in the magnetic field inclination resembling the spine and inter-spine structure in the photosphere. The observed inhomogeneity in the inclination of the chromospheric magnetic field on small-scales may play a role in driving small-scale chromospheric and transition region dynamics, such as, penumbral micro-jets (Katsukawa et al. 2007; Jurčák & Katsukawa 2008;

Reardon et al. 2013; Vissers et al. 2015; Tiwari et al. 2016) and transient bright dots (Tian et al. 2014). Scrutiny of this scenario requires a detailed analysis of the dynamics of the penumbral magnetic field in the chromosphere, and, of its coupling to the photosphere. A possible observational setup for this purpose would be similar to that presented in the current article but either in a sit-and-stare mode or with repetitive small raster scans (about  $3'' - 4''$  wide) parallel to penumbral filaments. These would be accompanied by images in Ca II H or K and Interface Region Imaging Spectrograph (IRIS, De Pontieu et al. 2014) data.

**Acknowledgements.** The 1.5-meter GREGOR solar telescope was built by a German consortium under the leadership of the Kiepenheuer-Institut für Sonnenphysik in Freiburg with the Leibniz-Institut für Astrophysik Potsdam, the Institut für Astrophysik Göttingen, and the Max-Planck-Institut für Sonnensystemforschung in Göttingen as partners, and with contributions by the Instituto de Astrofísica de Canarias and the Astronomical Institute of the Academy of Sciences of the Czech Republic. JJ acknowledges support from the CHROMOBS project funded by the Kunt and Alice Wallenberg Foundation. This work was partly supported by the BK21 plus program through the National Research Foundation (NRF) funded by the Ministry of Education of Korea. This study is supported by the European Commissions FP7 Capacities Programme under the Grant Agreement number 312495. The GRIS instrument was developed thanks to the support by the Spanish Ministry of Economy and Competitiveness through the project AYA2010-18029 (Solar Magnetism and Astrophysical Spectropolarimetry).

## References

- Andretta, V. & Jones, H. P. 1997, *ApJ*, 489, 375
- Avrett, E. H., Fontenla, J. M., & Loeser, R. 1994, in *IAU Symposium*, Vol. 154, *Infrared Solar Physics*, ed. D. M. Rabin, J. T. Jefferies, & C. Lindsey, 35
- Bard, S. & Carlsson, M. 2008, *ApJ*, 682, 1376
- Berkefeld, T., Schmidt, D., Soltau, D., von der Lüh, O., & Heidecke, F. 2012, *Astronomische Nachrichten*, 333, 863
- Berkefeld, T., Soltau, D., Schmidt, D., & von der Lüh, O. 2010, *Appl. Opt.*, 49, G155
- Borrero, J. M., Asensio Ramos, A., Collados, M., et al. 2016, *A&A* (submitted)
- Borrero, J. M. & Ichimoto, K. 2011, *Living Reviews in Solar Physics*, 8, 4
- Borrero, J. M., Lites, B. W., & Solanki, S. K. 2008, *A&A*, 481, L13
- Centeno, R., Trujillo Bueno, J., Uitenbroek, H., & Collados, M. 2008, *ApJ*, 677, 742
- Collados, M., Lagg, A., Díaz García, J. J., et al. 2007, in *Astronomical Society of the Pacific Conference Series*, Vol. 368, *The Physics of Chromospheric Plasmas*, ed. P. Heinzel, I. Dorotović, & R. J. Rutten, 611
- Collados, M., López, R., Páez, E., et al. 2012, *Astronomische Nachrichten*, 333, 872
- Cuperman, S., Li, J., & Semel, M. 1992, *A&A*, 265, 296
- De Pontieu, B., Title, A. M., Lemen, J. R., et al. 2014, *Sol. Phys.*, 289, 2733
- Esteban Pozuelo, S., Bellot Rubio, L. R., & de la Cruz Rodríguez, J. 2015, *ApJ*, 803, 93
- Franz, M., Collados, M., Bethge, C., et al. 2016, *A&A* (submitted)
- Franz, M. & Schlichenmaier, R. 2013, *A&A*, 550, A97
- Frutiger, C., Solanki, S. K., Fligge, M., & Bruls, J. H. M. J. 2000, *A&A*, 358, 1109
- Joshi, J. 2014, PhD thesis, Technische Universität Braunschweig, ISBN 978-3-944072-01-2, uni-edition GmbH 2014
- Joshi, J., Lagg, A., Hirzberger, J., & Solanki, S. K. 2016a, *A&A* (in preparation)
- Joshi, J., Lagg, A., Hirzberger, J., Solanki, S. K., & Tiwari, S. K. 2016b, *A&A* (submitted)
- Joshi, J., Pietarila, A., Hirzberger, J., et al. 2011, *ApJ*, 734, L18
- Jurčák, J. & Katsukawa, Y. 2008, *A&A*, 488, L33
- Katsukawa, Y., Berger, T. E., Ichimoto, K., et al. 2007, *Science*, 318, 1594
- Kuckein, C., Martínez Pillet, V., & Centeno, R. 2012, *A&A*, 539, A131
- Lagg, A., Ishikawa, R., Merenda, L., et al. 2009, in *Astronomical Society of the Pacific Conference Series*, Vol. 415, *The Second Hinode Science Meeting: Beyond Discovery-Toward Understanding*, ed. B. Lites, M. Cheung, T. Magara, J. Mariska, & K. Reeves, 327
- Lagg, A., Woch, J., Krupp, N., & Solanki, S. K. 2004, *A&A*, 414, 1109
- Langhans, K., Scharmer, G. B., Kiselman, D., Löfdahl, M. G., & Berger, T. E. 2005, *A&A*, 436, 1087
- Leenaarts, J., Golding, T., Carlsson, M., Libbrecht, T., & Joshi, J. 2016, *A&A* (submitted)
- Lites, B. W., Elmore, D. F., Seagraves, P., & Skumanich, A. P. 1993, *ApJ*, 418, 928
- Livingston, W. & Wallace, L. 1991, *An atlas of the solar spectrum in the infrared from 1850 to 9000 cm<sup>-1</sup> (1.1 to 5.4 micrometer)*, NSO Technical Report, National Solar Observatory
- Magara, T. 2010, *ApJ*, 715, L40
- Martínez Pillet, V. 2000, *A&A*, 361, 734
- Reardon, K., Tritschler, A., & Katsukawa, Y. 2013, *ApJ*, 779, 143
- Rempel, M. & Schlichenmaier, R. 2011, *Living Reviews in Solar Physics*, 8, 3
- Rüedi, I., Solanki, S. K., & Livingston, W. C. 1995, *A&A*, 293, 252
- Ruiz Cobo, B. & Asensio Ramos, A. 2013, *A&A*, 549, L4
- Sakurai, T., Makita, M., & Shibasaki, K. 1985, in *Theo. Prob. High Resolution Solar Physics*, ed. H. U. Schmidt, 313
- Schad, T. A., Penn, M. J., Lin, H., & Tritschler, A. 2015, *Sol. Phys.*, 290, 1607
- Scharmer, G. B., de la Cruz Rodríguez, J., Sütterlin, P., & Henriques, V. M. J. 2013, *A&A*, 553, A63
- Scharmer, G. B. & Henriques, V. M. J. 2012, *A&A*, 540, A19
- Scharmer, G. B., Henriques, V. M. J., Kiselman, D., & de la Cruz Rodríguez, J. 2011, *Science*, 333, 316
- Schmidt, W., Hofmann, A., Balthasar, H., Tarbell, T. D., & Frank, Z. A. 1992, *A&A*, 264, L27
- Schmidt, W., von der Lüh, O., Volkmer, R., et al. 2012, *Astronomische Nachrichten*, 333, 796
- Solanki, S. K. 1987, PhD thesis, PhD thesis No. 8309, ETH, Zürich
- Solanki, S. K. 2003, *A&A Rev.*, 11, 153
- Solanki, S. K. & Montavon, C. A. P. 1993, *A&A*, 275, 283
- Tian, H., Kleint, L., Peter, H., et al. 2014, *ApJ*, 790, L29
- Title, A. M., Frank, Z. A., Shine, R. A., et al. 1993, *ApJ*, 403, 780
- Tiwari, S. K., Moore, R. L., Winebarger, A. R., & Alpert, S. E. 2016, *ApJ*, 816, 92
- Tiwari, S. K., van Noort, M., Lagg, A., & Solanki, S. K. 2013, *A&A*, 557, A25
- Tiwari, S. K., van Noort, M., Solanki, S. K., & Lagg, A. 2015, *A&A*, 583, A119
- van Noort, M., Lagg, A., Tiwari, S. K., & Solanki, S. K. 2013, *A&A*, 557, A24
- Vissers, G. J. M., Rouppe van der Voort, L. H. M., & Carlsson, M. 2015, *ApJ*, 811, L33
- Wallace, L., Hinkle, K., & Livingston, W. C. 1993, *An atlas of the photospheric spectrum from 8900 to 13600 cm<sup>-1</sup> (7350 to 11230 Å)*, NSO Technical Report 93-001, National Solar Observatory
- Wilkinson, L. K., Emslie, G. A., & Gary, G. A. 1989, *Sol. Phys.*, 119, 77